

# Iteratively decoded magic state distillation

Kwok Ho Wan <sup>1,2,\*</sup>

<sup>1</sup>*Universal Quantum Ltd, Gemini House, Haywards Heath, RH16 1XQ, United Kingdom*

<sup>2</sup>*Blackett Laboratory, Imperial College London, London SW7 2AZ, United Kingdom*

(Dated: January 28, 2026)

We present numerical simulation results for the 7-to-1 and 15-to-1 state distillation circuits, constructed using transversal CNOTs acting on multiple surface code patches. The distillation circuits are decoded iteratively using the method outlined in [arXiv:2407.20976]. We show that, with a re-configurable qubit architecture, we can perform fast magic state distillation in  $\sim \mathcal{O}(1)$  code cycles. We confirm that both circuits suppress an injected input error rate  $p$  to  $\mathcal{O}(p^3)$  in the presence of additional circuit-level noise. We also outline how ZX-calculus and Pauli webs can be used to benchmark stabiliser proxies for these distillation circuits.

## I. INTRODUCTION

The surface code [1–3] is a strong candidate for large-scale fault-tolerant quantum computation. Every Clifford gate ( $H, S, \text{CNOT}$ ) on the surface code permits a transversal implementation given a re-configurable hardware architecture or flying qubits [4], while the non-Clifford  $T = \begin{pmatrix} 1 & 0 \\ 0 & e^{i\frac{\pi}{4}} \end{pmatrix}$  gate cannot be implemented transversally [5, 6]. One approach to bypass this restriction is to perform  $T$  gates via gate teleportation. This is achieved by consuming the magic state:  $|T\rangle \propto |0\rangle + e^{i\frac{\pi}{4}}|1\rangle$  in the process.

Before the consumption of  $|T\rangle$  state is possible, magic state injection techniques are needed to encode faulty logical  $|T\rangle$  states from physical  $|T\rangle$  states [7–10]. Then, the 15-to-1 distillation protocol (also known as distillation factory) is used to output a higher quality logical  $|T\rangle$  state [11–13]. Similarly, another resource state:  $|Y\rangle \propto |0\rangle + i|1\rangle$  can also be injected, distilled using the 7-to-1 distillation protocol [4, 14, 15] and consumed in a similar manner to perform the  $S = \begin{pmatrix} 1 & 0 \\ 0 & i \end{pmatrix}$  gate. Lower overhead methods of initialising a high quality logical  $|Y\rangle$  state has recently become available [16], this may make the 7-to-1 distillation protocol obsolete. Alternatively, the transversal logical  $S$  gate can be implemented with physical  $S, S^\dagger$  and CZ gates on the surface code [4, 17, 18]. Nevertheless, studying the 7-to-1 protocol can be insightful as the 7-to-1 and 15-to-1 protocols have many parallels.

In general, state distillation aims to use multiple faulty resource states with input error  $p$ , and output a higher quality  $|T/Y\rangle$  state with suppressed output error rate of  $p_{\text{out}} = \mathcal{O}(p^3)$ . To leading order in  $p$ ,  $p \xrightarrow{15\text{-to-1}} 35p^3$  [11, 12] and  $p \xrightarrow{7\text{-to-1}} 7p^3$  [14, 15]

Historically, state distillation protocols are the leading contributor to the spacetime volume footprint of a fault-tolerant quantum computer [3, 14, 15]. Magic state dis-

tillation using lattice surgery based techniques requires a spacetime overhead of  $\mathcal{O}(d^3)$  qubit-cycles (physical data qubits  $\times$  code cycles), where  $d$  is the distance of the surface code. This spacetime overhead had drastically decreased from  $\mathcal{O}(1500d^3)$  [14, 15] to  $\mathcal{O}(624d^3)$  [3] or  $\mathcal{O}(396d^3)$  for the  $|CCZ\rangle$  state distillation factory [19] [20]. However, all of the above mentioned state distillation schemes will output one  $|T\rangle$  state (2  $|T\rangle$  states for the  $|CCZ\rangle$  factory) every  $5.5d$  to  $6.5d$  code cycles. For larger code distances, the time complexity cost will pose run-time challenges for trapped-ion and neutral-atom platforms, where the code cycle times are considerably slower, in the kHz regime [21–24] compared to MHz in superconducting platforms [25].

To bridge this three orders of magnitude gap in code cycle rate [4, 24, 26–30], we use the iterative transversal CNOT decoding technique from [31] to collapse the time complexity of both the 15-to-1 and 7-to-1 distillation protocols to  $\mathcal{O}(1)$ , removing its dependence on  $d$ . We numerically confirm the 7-to-1 distillation simulation results from [4], without the need for a hyper-edge decoding graph or most-likely error (MLE) decoders [4, 30]. In our approach, each surface code patch is decoded separately before iteratively propagating Pauli-frames from each corresponding patch [31]. Furthermore, we extended our approach to numerically characterise the 15-to-1 distillation protocol. We confirm the  $p \rightarrow \mathcal{O}(p^3)$  scaling in both distillation protocols using stabiliser proxies.

We claim that the 7-to-1 and 15-to-1 distillation protocols can be implemented with  $8d^2 \times 5 + 7d^2 = 47d^2$  and  $16d^2 \times 6 + 15d^2 = 111d^2$  qubit-cycles respectively in re-configurable hardware platforms using the transversal CNOT decoder from [31]. These reported costs follow the convention from [32] and do not include both physical measurement ancilla qubits [33] or the magic state injection cost. Our results provide a factor  $d$  speed up for both distillation schemes compared to lattice surgery alternatives. In our simulations, we assume minimal shuttling and transversal CNOT errors. These assumptions will be further explored in works in preparation [34].

This paper is structured as follows. Firstly, we introduce the 7-to-1 and 15-to-1 distillation circuits in section II. Then, we present our contributions in section III, sim-

\* ((initials))1496@((9.81))mail.com

ulating each distillation circuit with multiple surface code patches entangled with transversal CNOTs. Finally, we provide discussions and future directions in the last section.

## II. STATE DISTILLATION PROTOCOLS

In this section, we review the 7-to-1 and 15-to-1 distillation protocols and their underlying quantum error correcting codes: Steane and Reed-Muller code. We then discuss the post-selection protocol required in both distillation protocols to output an error suppressed distilled state.

The 15-to-1  $|T\rangle$  and 7-to-1  $|Y\rangle$  state distillation circuits are CNOT circuits followed by a resource state consumption stage, measurement and post-selection. They rely on the ability to perform specific gates via gate teleportation. This involves consuming many copies of faulty  $|T\rangle$  ( $|Y\rangle$ ) states and post-selecting measurement results to detect errors. One simple error is  $Z \cdot T$  ( $Z \cdot Y$ ) performed on the output state instead of  $T$  ( $Y$ ).

The circuits in equation 1 show consumption of  $|-\rangle \propto |0\rangle - |1\rangle$ ,  $|Y\rangle$  and  $|T\rangle$  states to perform a  $Z$ ,  $S$  and  $T$  gate respectively, up to measurement-conditioned Clifford byproducts [35].

$$\begin{array}{l}
 \begin{array}{c}
 |\phi\rangle \text{---} \bullet \text{---} (-1)^n Z |\phi\rangle \\
 |-\rangle \text{---} \oplus \text{---} \boxed{\text{meter}} = n
 \end{array} \\
 \begin{array}{c}
 |\phi\rangle \text{---} \bullet \text{---} Z^n S |\phi\rangle \\
 |Y\rangle \text{---} \oplus \text{---} \boxed{\text{meter}} = n
 \end{array} \\
 \begin{array}{c}
 |\phi\rangle \text{---} \bullet \text{---} (S^\dagger)^n T |\phi\rangle \\
 |T\rangle \text{---} \oplus \text{---} \boxed{\text{meter}} = n
 \end{array}
 \end{array} \quad (1)$$

The 7-to-1  $|Y\rangle$  and 15-to-1  $|T\rangle$  distillation protocols consume resource states needed to perform the  $S$  and  $T$  gates respectively. However, they also distill all resource states that perform integer powers of  $S$  and  $T$  respectively [13, 15]. The tuples, (resource state, gate by teleportation), below in equation 2 show what can be distilled by each protocol:

$$\begin{array}{l}
 \text{7-to-1 protocol: } \left\{ (|-\rangle, Z), (|Y\rangle, S) \right\} \\
 \text{15-to-1 protocol: } \left\{ (|-\rangle, Z), (|Y\rangle, S), (|T\rangle, T) \right\}.
 \end{array} \quad (2)$$

In order to investigate the effectiveness of either distillation circuits, we looked at the stabiliser proxy of  $|-\rangle$  state distillation using the 7-to-1 and 15-to-1 circuits in our numerical simulations. In practice, simple transversal implementation of the logical  $Z$  gate exists for surface code and will never realistically be performed in this manner with gate teleportation. We assume numerical results from  $|-\rangle$  state distillation provide an order-of-magnitude estimation to the actual performance of  $|Y\rangle$  or  $|T\rangle$  state distillation. The true performance of any non-Clifford

state distillation will have to be confirmed through experimental demonstrations on real hardware [10, 36].

We will now provide some background on the 7-to-1 and 15-to-1 distillation circuits along with the post-selection required to achieve the cubic error suppression. Unless otherwise specified, all the gates and measurements from this point onwards are understood to be in the surface code logical basis.

### A. 7-to-1 distillation protocol

The 7-to-1 distillation protocol relies on the  $[[7, 1, 3]]$  Steane code's transversal  $S$  gate,  $S_{\text{Steane}}$  [37]. Figure 1 shows the Tanner graph of the self-dual Steane code. The encoding qubits are arranged as circular nodes, lying on the corners, mid-points and centroid of an equilateral triangle. The rectangular nodes are stabilisers ( $X$  or  $Z$ ) of the code connected to qubits involved in each stabiliser check.

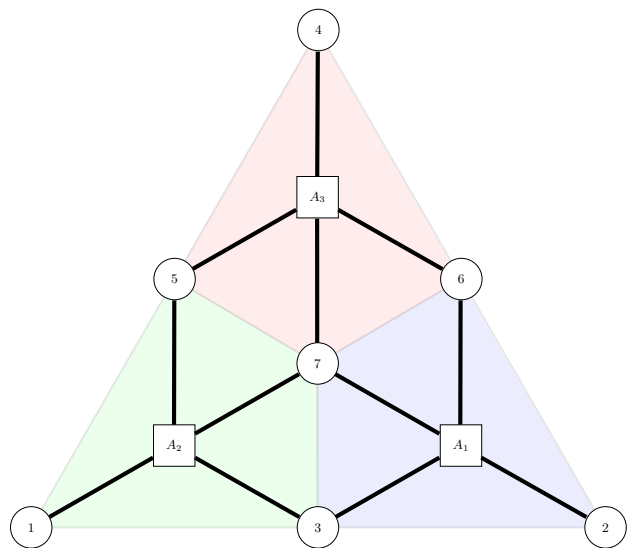


Figure 1. Tanner graph for the Steane code, encoded using 7 qubits arranged in the usual geometric manner on a triangle, rectangular nodes:  $\{A_0, A_1, A_2\}$  are the self-dual  $X$  or  $Z$  stabiliser checks, while circular nodes 1-7 are the qubit labels.

We take the 7-to-1 distillation circuit (figure 2) from [4] with the first and fourth redundant transversal CNOTs removed. There is a one-to-one mapping of qubit labels between this circuit and qubit labels on the triangle in figure 1. The additional 0<sup>th</sup> qubit in the circuit is the output subsystem of this distillation circuit.

The 7-to-1 distillation circuit consists of 3 parallel layers of transversal CNOTs (separated by blue dotted lines in figure 2) performed on surface code patches initialised in the  $|+\rangle$  or  $|0\rangle$  state, followed by  $|Y\rangle$  state consumption that perform  $S$  gates on patches 1 to 7, before measuring out the corresponding patches in the  $X$  or  $Z$  basis. Prior to the state consumption and readout stage, this circuit encodes the state stabilised by:

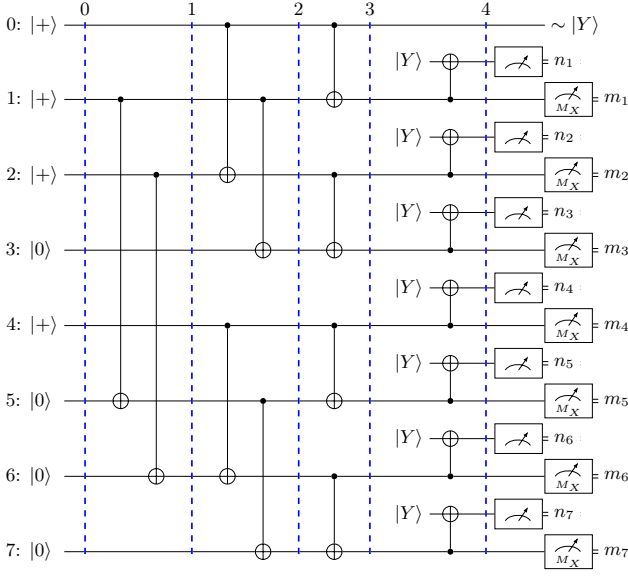


Figure 2. The 7-to-1 distillation circuit from [4] with the first and fourth redundant CNOTs removed as the CNOTs were acting on either  $|+, +\rangle$  or  $|0, 0\rangle$ . A single round of syndrome extraction is inserted at every time step indicated by blue dotted lines in the surface code simulations.

$$\left\langle \overbrace{X_0 \prod_{j=1}^7 X_j}^{\bar{X}_{\text{Steane}}}, \underbrace{Z_0 \prod_{j=1}^7 Z_j}_{\bar{Z}_{\text{Steane}}} \right\rangle \cup \mathcal{G}_{\text{Steane}}, \quad (3)$$

$$\mathcal{G}_{\text{Steane}} = \left\langle X_1 X_3 X_5 X_7, X_2 X_3 X_6 X_7, X_4 X_5 X_6 X_7, Z_1 Z_3 Z_5 Z_7, Z_2 Z_3 Z_6 Z_7, Z_4 Z_5 Z_6 Z_7 \right\rangle, \quad (4)$$

where  $\mathcal{G}_{\text{Steane}}$  consists of Steane code stabilisers and  $\bar{X}_{\text{Steane}}$ ,  $\bar{Z}_{\text{Steane}}$  are the  $X$ ,  $Z$  logical operators of the Steane code. Equation 3 is equivalent to a Bell state of the 0<sup>th</sup> surface code patch entangled with the Steane code encoded with patches 1 to 7. The state consumption stage uses 7  $|Y\rangle$  states to perform an  $S$  gate on surface code patches 1 to 7 through measurements in the  $Z$  basis (binary results  $n_j$ ). This is equivalent to performing a  $\bar{S}_{\text{Steane}}$  gate at the Steane code level. After the  $Z$  measurements, the resulting state is stabilised by:

$$\begin{aligned} & \left\langle (-Y_0) \bar{X}_{\text{Steane}} \cdot (-1)^{\sum_{k=1}^7 n_k}, \right. \\ & X_1 X_3 X_5 X_7 (-1)^{n_1+n_3+n_5+n_7}, \\ & X_2 X_3 X_6 X_7 (-1)^{n_2+n_3+n_6+n_7}, \\ & X_4 X_5 X_6 X_7 (-1)^{n_4+n_5+n_6+n_7} \left. \right\rangle \\ & \cup Z \text{ type operators.} \end{aligned} \quad (5)$$

Next, perform the  $X$  basis measurements (binary results  $m_j$ ), the output state is stabilised by:

$$\left\langle Y_0 \cdot (-1)^{(1+\sum_{k=1}^7 n_k+m_k)} \right\rangle. \quad (6)$$

Note that we have managed to force the 0<sup>th</sup> output surface code patch to be stabilised by  $Y_0$  up to a  $\pm$  sign, depending on measurement results.

However, the input resource states or the distillation circuit can be faulty. The measurements results in the  $X$  and  $Z$  basis ( $m_j, n_j \in \{0, 1\}$ ) are used to construct the Steane code stabilisers. These stabiliser measurement results will be used to post-select and identify erroneous output states.

See detailed discussion in [15] on the 7-to-1 post-selection procedure. In summary:

1. Construct the three weight-4  $X$  type Steane code stabilisers:

$$\begin{aligned} X_1 X_3 X_5 X_7 &= \prod_{l \in \{n, m\}} (-1)^{l_1+l_3+l_5+l_7} \\ X_2 X_3 X_6 X_7 &= \prod_{l \in \{n, m\}} (-1)^{l_2+l_3+l_6+l_7} \\ X_4 X_5 X_6 X_7 &= \prod_{l \in \{n, m\}} (-1)^{l_4+l_5+l_6+l_7}, \end{aligned} \quad (7)$$

with the measurement results  $(m_j, n_j)$ , post-select on shots where all three stabilisers return the trivial result, i.e.  $X_1 X_3 X_5 X_7 = X_2 X_3 X_6 X_7 = X_4 X_5 X_6 X_7 = 1$ .

2. If  $\prod_{j=1}^7 (-1)^{n_j+m_j} = 1$ , there is an additional  $Z_0$  Clifford offset to the 0<sup>th</sup> subsystem's Pauli-frame, that needs to be tracked (notice the sign of  $Y_0$  in equation 6).

Successful post-selection outputs a  $|Y\rangle$  state with suppressed error:  $p_{\text{out}} = \mathcal{O}(7p^3)$ , given  $|Y\rangle$  resource states with input error rate  $p$  and a perfect distillation circuit. Assuming an error-free 7-to-1 distillation circuit, the full expression [4] for  $p_{\text{out}}$  is:

$$p_{\text{out}} = \frac{7p^3(1-p)^4 + p^7}{p^7 + (1-p)^7 + 7(1-p)^3p^4 + 7(1-p)^4p^3}. \quad (8)$$

Due to the post-selection procedure, a certain number of shots/experiments will be discarded. The number of shots discarded should be proportional to  $\mathcal{O}(7p)$  at low error rates [4]. We will discuss simulation results concerning the 7-to-1 distillation circuit in section III and confirming its error suppression and discard ratio scaling under circuit-level noise.

## B. 15-to-1 distillation protocol

The 15-to-1 distillation protocol is enabled by the [[15, 1, 3]] Reed-Muller code [38], which allows for a

transversal  $T$  gate. This code has a geometric interpretation of qubits lying on the vertices of a tetrahedron complex, cellulated by four identical 6-sided polyhedron cells, in the configuration shown in figure 3. This code has four weight-8  $X$  stabiliser checks specified by the cells of this tetrahedron. One example of a weight-8  $X$  stabiliser check is shown in figure 4.

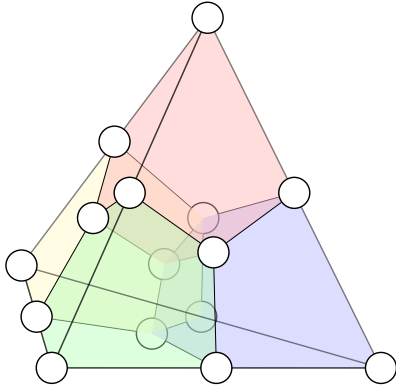


Figure 3. The  $[[15, 1, 3]]$  Reed-Muller code's geometric representation with encoding qubits as circular nodes, rectangular stabiliser check nodes and its edges are excluded for representation purposes.

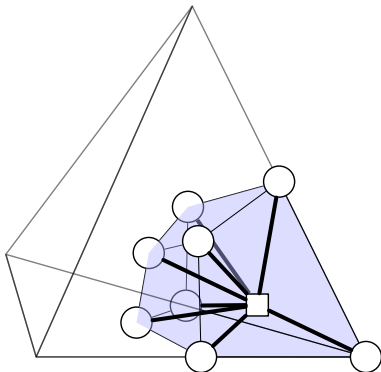


Figure 4. One of the four weight-8  $X$  stabiliser check cells in the  $[[15, 1, 3]]$  Reed-Muller code with the rectangular stabiliser check node explicitly shown.

The circuit in figure 5 is a construction of the 15-to-1 distillation protocol [39]. This circuit consists of 16 surface code patches initialised in the  $|+\rangle$  or  $|0\rangle$  state, before going through 4 parallel layers of CNOTs. This CNOT circuit (up until the blue dotted line labelled 4 in figure 5) generates a  $r = 1$  Reed-Muller state,  $|QMR_r\rangle$ , from [39]. This 16 patch  $|QMR_r\rangle$  state is a Bell state of the  $0^{\text{th}}$  surface code patch entangled with the Reed-Muller code, stabilised by:

$$\langle X_0 \bar{X}_{\text{RM}}, Z_0 \bar{Z}_{\text{RM}} \rangle \cup \mathcal{G}_{\text{RM}}. \quad (9)$$

The generators  $\mathcal{G}_{\text{RM}}$  are the Reed-Muller code stabilisers

and  $\bar{X}_{\text{RM}}$  and  $\bar{Z}_{\text{RM}}$  are the logical operators of the Reed-Muller code:

$$\bar{X}_{\text{RM}} = \prod_{j \in \text{Face}} X_j = \text{[Diagram of tetrahedron with red nodes on faces]} \quad , \quad (10)$$

$$\bar{Z}_{\text{RM}} = \prod_{j \in \text{Edge}} Z_j = \text{[Diagram of tetrahedron with blue nodes on edges]} \quad . \quad (11)$$

The operators  $\bar{X}_{\text{RM}}$  and  $\bar{Z}_{\text{RM}}$  are any weight-7  $X$ -faces and any weight-3  $Z$ -edge strings of the entire tetrahedron [38].

After the CNOT circuit, a logical  $T$  gate is performed at the Reed-Muller code level via consuming 15 surface code  $|T\rangle$  states and measurements in the  $Z$  basis. Conditioned on the  $Z$  basis measurements,  $S$  gate(s) will be performed on the appropriate patch(es). This is followed by measurements in the  $X$  basis, in order to construct all four weight-8  $X$  stabiliser checks of the Reed-Muller code:

$$\begin{aligned} & \langle X_1 X_3 X_5 X_7 X_9 X_{11} X_{13} X_{15}, \\ & X_2 X_3 X_6 X_7 X_{10} X_{11} X_{14} X_{15}, \\ & X_4 X_5 X_6 X_7 X_{12} X_{13} X_{14} X_{15}, \\ & X_8 X_9 X_{10} X_{11} X_{12} X_{13} X_{14} X_{15} \rangle. \end{aligned} \quad (12)$$

The measurement results are then post-selected upon the trivial result on all four stabiliser checks. The value of  $\bar{X}_{\text{RM}}$ , given by  $M(\bar{X}_{\text{RM}})$  must also be constructed from these measurement results, as the final gate implemented on the  $0^{\text{th}}$  patch is  $T^{3-2M(\bar{X}_{\text{RM}})}$  [39].

Given 15 faulty  $|T\rangle$  states with input error probability  $p$ , the error-free 15-to-1 distillation circuit suppresses the error of the output state to  $\mathcal{O}(35p^3)$ , with the full expression below [11]:

$$p_{\text{out}} = \frac{1 - 15(1 - 2p)^7 + 15(1 - 2p)^8 - (1 - 2p)^{15}}{2(1 + 15(1 - 2p)^8)}. \quad (13)$$

Similar to the 7-to-1 protocol, the post-selection procedure should discard  $\mathcal{O}(15p)$  shots at low input error rates [39]. Both the error suppression and discard ratio scaling will be numerically confirmed in section III later. Note that the 15-to-1  $|-\rangle$  state distillation does not require feed-forward  $S$  gates at the surface code level. This simplifies the numerical simulations, if a  $|-\rangle$  state is consumed in place of a  $|T\rangle$  state.

### III. SURFACE CODE SIMULATIONS

In the following section, we present our various numerical findings on the performance of both distillation

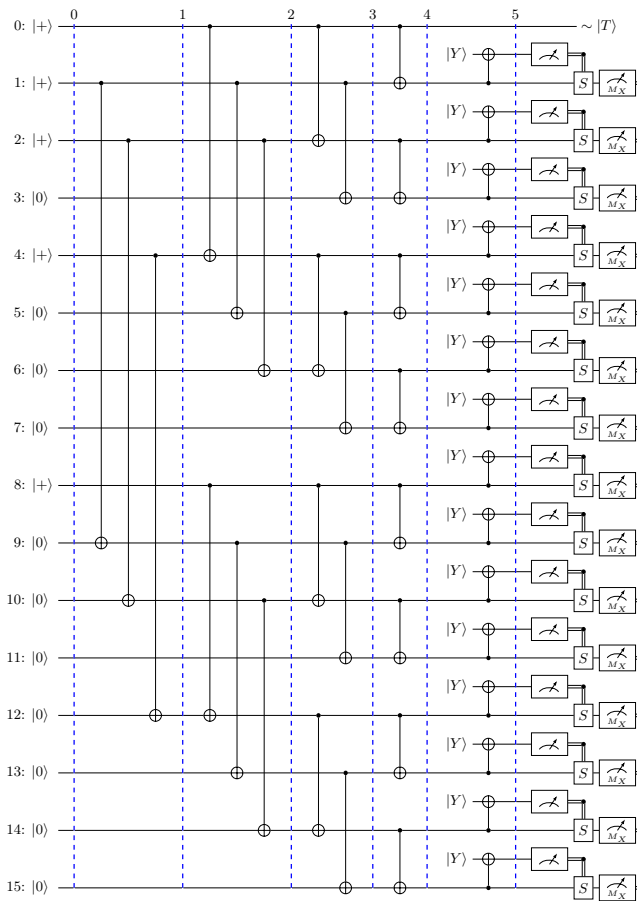


Figure 5. The 15-to-1 ( $|T\rangle$ ) distillation circuit from [39] with all the redundant CNOTs removed. A single round of syndrome extraction is inserted at every time step indicated by blue dotted lines in the surface code simulations.

circuits. One of the aims of this paper is to investigate whether the distillation error suppression scaling ( $p \rightarrow \mathcal{O}(p^3)$ ) holds using surface code patches entangled with transversal CNOTs. We employ the iterative decoding scheme from [31] to decode the entire CNOT circuits in figure 2 and 5. In order to characterise the performance of each protocol, we distil the logical  $|-\rangle$  state as a stabiliser proxy for the performance of either distillation circuits. In our simulations, we assume the following [31]:

1. Error-free and instantaneous transversal CNOTs (transversal CNOT errors can be subsumed into a marginally higher circuit-level noise).
2. Standard SD6 circuit-level depolarising noise model [40, 41] on all gates except the resource state initialisation errors.
3. Artificial injection of  $Z$  input errors [4] (with probability  $p$ ) on all resource states to be consumed.

Interestingly, one can perform an inplace  $Y$  basis measurement on the surface code [10, 16, 42], this can also

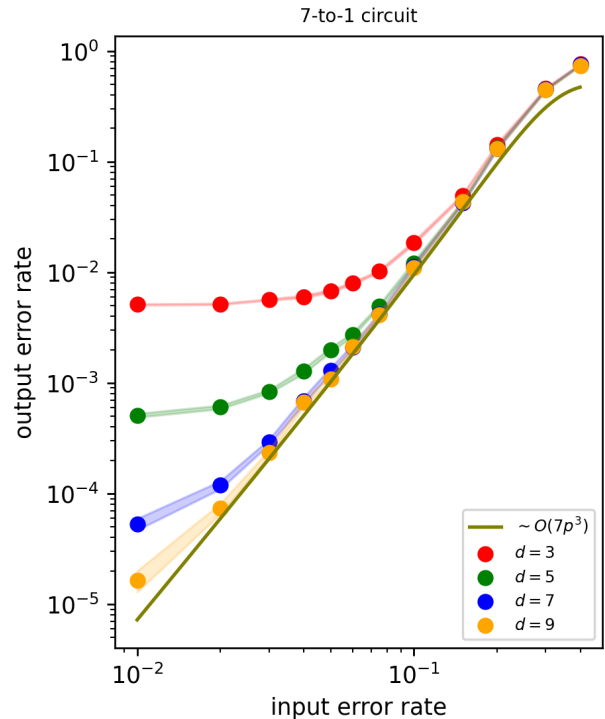


Figure 6. Surface code simulations of the 7-to-1 distillation output error rate. The output error scaling:  $\mathcal{O}(7p^3)$  is confirmed across distances  $d \in \{3, 5, 7, 9\}$  at 0.1% circuit-level noise.

be used to benchmark both distillation protocols [34].

We demonstrate that the iterative decoding scheme from [31] can perform well in the context of state distillation. Furthermore, we propose a time complexity speed up given a re-configurable qubit platform such as trapped-ions [28, 29] with the ability to perform long-range two qubit gates.

We use Stim [43] to construct and sample the logical circuits from figures 2 and 5, we decode each surface code patch separately using PyMatching [44] and propagate the Pauli-frames accordingly when a transversal logical CNOT is applied. No more than 3 global iterations of the algorithm provided in [31] were needed in all of the following simulations. A single round of syndrome extraction is inserted on all the logical qubits at every time step labelled with blue dotted lines in figures 2 and 5. We benchmark the circuits by computing the stabiliser proxy of distilling a logical  $|-\rangle$  state. We treat this as an order-of-magnitude estimate for the true performance of state distillation when logical  $|Y\rangle$  or  $|T\rangle$  states are involved.

The output error rates for the 7-to-1 circuit (figure 6) and the 15-to-1 circuit (figure 7) match the expected  $\mathcal{O}(p^3)$  scaling well. We simulated the 7-to-1 circuit from [4], however we noticed that the first and fourth CNOTs applied in [4] are redundant as they act on either  $|0, 0\rangle$  or  $|+, +\rangle$ , hence these gates are removed in our simulations. We confirmed the single level distillation factory

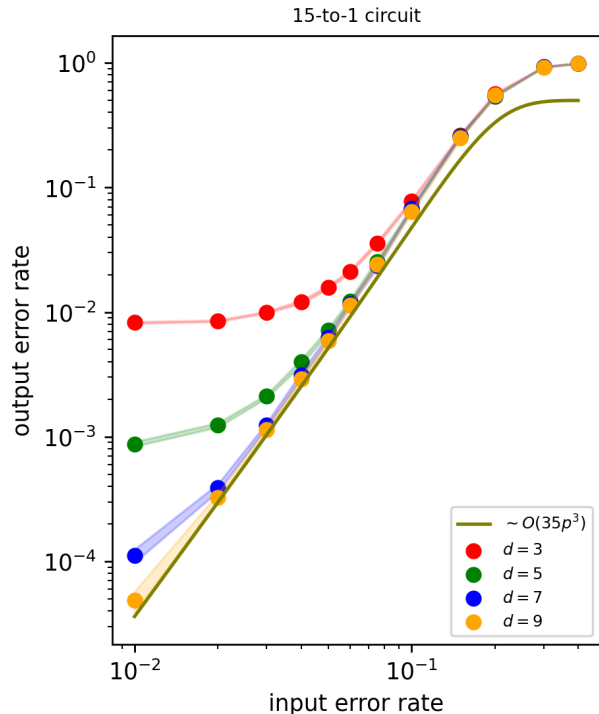


Figure 7. Surface code simulations of the 15-to-1 distillation output error rate. The output error scaling:  $\mathcal{O}(35p^3)$  is confirmed across distances  $d \in \{3, 5, 7, 9\}$  at 0.1% circuit-level noise.

results from [4] at circuit-level noise  $p_{\text{circuit}} = 0.1\%$ . We noticed similar deviation from the zero circuit-level noise curve over a range of distances  $d \in \{3, 5, 7, 9\}$ . Furthermore, we also notice similar deviations in our 15-to-1 circuit simulations. This is due to circuit-level noise imperfections similar to the findings from [4]. For different surface code distances, the output error rate seems to plateau at specific values. Further work is needed to extract the behaviour between distance vs plateau value with more computational power at lower input error rates and higher distances. Additionally, we also confirm the discard ratios at the post-selection stage of both distillation protocols at low input error rates, as shown in figure 8. In addition to the previous numerical simulations, we also computed the overall logical fidelity of the pure CNOT sub-circuit component of either distillation protocols. The logical error rate in figure 9 is defined to be the transversal CNOT sub-circuit logical failure rate benchmarked using stabiliser flow[45]/Pauli web [46–49]. See the appendices for discussions on using Pauli webs to benchmark these circuits. Close agreement of logical error rates compared to the equivalent idling memory experiment is observed in both distillation CNOT sub-circuits (figure 9).

All the above numerical evidences suggest that the distillation circuits can suppress errors with the correct scaling in the presence of circuit-level noise when decoded

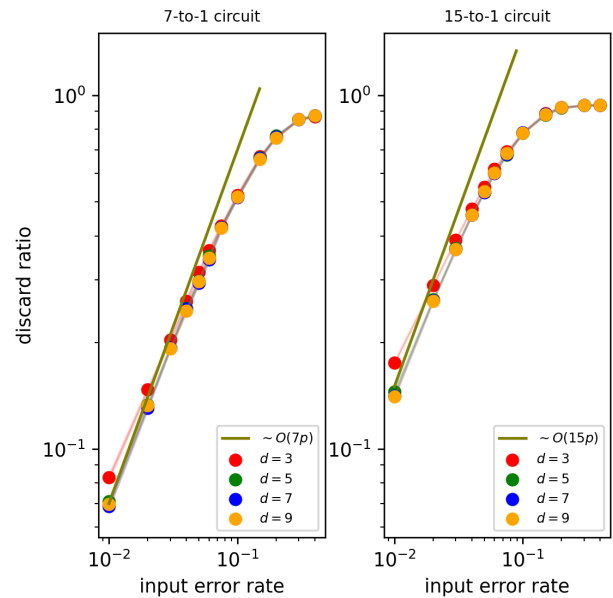


Figure 8. The discard ratio of the 7-to-1 circuit (left) and 15-to-1 circuit (right) stemming from the surface code simulations. We confirm the discard ratio of  $\mathcal{O}(7p)$  and  $\mathcal{O}(15p)$  at low input error rate  $p$  for both distillation protocol.

using [31]. In re-configurable hardware platforms with minimal shuttling fidelity degradation, the 15-to-1 distillation protocol [50] can be performed with 6 code cycles, 15 logical qubits and 15  $|T\rangle$  states to be consumed. This implies a total qubit-cycle of  $16d^2 \times 6 + 15d^2 = 111d^2$  excluding physical ancilla qubits and magic state injection cost. Likewise, the 7-to-1 distillation protocol spacetime cost is:  $8d^2 \times 5 + 7d^2 = 47d^2$  qubit-cycles with similar constructions.

#### IV. DISCUSSIONS AND OUTLOOK

The numerical simulation results in this manuscript address the feasibility of using long-range transversal CNOT operations to perform magic state distillation with the surface code.

The crux of this study is to confirm the error suppression scaling:  $p \xrightarrow{15\text{-to-1}} 35p^3$  and  $p \xrightarrow{7\text{-to-1}} 7p^3$ , under circuit-level noise with injected  $Z$  input logical error of strength  $p$ . Our results show that a single-level distillation factory can indeed suppress error, and distill resource states when paired with the decoder from [31]. We remark that each surface code patch is decoded separately, with appropriate propagation of Pauli-frames. No more than 3 global rounds of iterative decoding is needed in either distillation circuit simulations. Our numerical results suggest that fast  $\mathcal{O}(1)$  code cycles magic state distillation can be made possible on re-configurable qubit platforms. However, the true magic state distillation performance will have to be confirmed in experiments

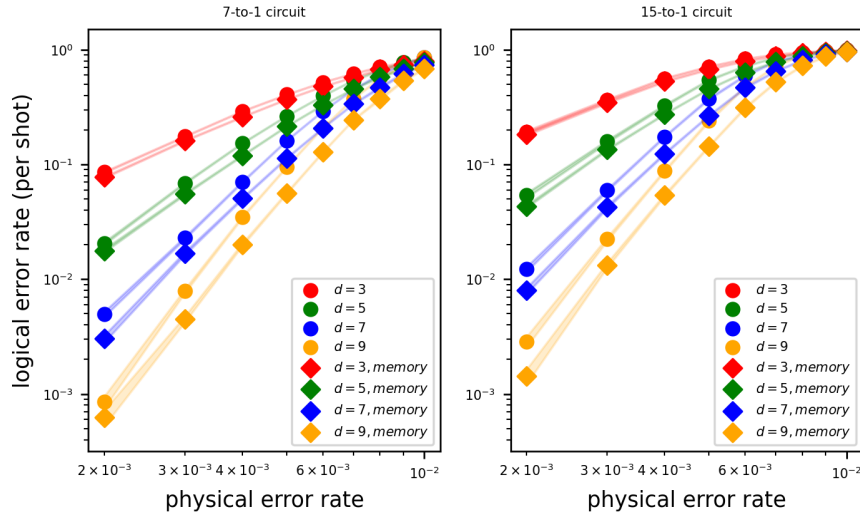


Figure 9. Logical error rate comparisons of the 7-to-1 (left) and 15-to-1 (right) pure CNOT sub-circuits against an equivalent memory experiment with the same number of syndrome extraction rounds.

[10, 42] as no efficient large scale non-Clifford simulation algorithm exists [51].

This work provides a step towards realistic implementation of time-optimal magic state distillation on reconfigurable hardware architectures. Future works on implementing an inplace  $Y$  basis measurement will allow for more accurate performance benchmark of both factories. In addition, analysis of hardware realistic connectivity error models is under preparation [34].

Recent works on magic state cultivation [10, 52–55] promises high quality injected (‘cultivated’) magic state with logical error rate as low as  $2 \times 10^{-9}$  and expected spacetime volume of  $5 \times 10^3$  qubit-cycles at 0.1% circuit-level noise [52]. This may potentially make multi-level magic state distillation obsolete. However, many fault-tolerant quantum algorithms require T-count greater than  $\frac{1}{2 \times 10^{-9}} = 5 \times 10^8$  [56]. Single-level magic state distillation might still be vital in suppressing error rates from

$2 \times 10^{-9} \xrightarrow{15\text{-to-1}} 2.8 \times 10^{-25}$ . Incorporating an end-to-end analysis of magic state cultivation followed by transversal CNOT enabled magic state distillation is a fruitful topic to study.

## ACKNOWLEDGMENTS

We acknowledge discussions with Zhenghao Zhong on Pauli webs and Mark Webber on early manuscript feedback. We want to thank our colleagues at Universal Quantum Ltd for their support. The numerical simulations were performed on a 2023 version Dell XPS17 laptop with an Intel Core i7-12700H (14 cores) processor and 64 GB of physical memory (RAM). The tikzpicture code used to construct the tetrahedron can be found in [57]. Most of the ZX-diagrams in the appendices were generated using pyzx [58].

- 
- [1] E. Dennis, A. Kitaev, A. Landahl, and J. Preskill, *Journal of Mathematical Physics* **43**, 4452–4505 (2002).
- [2] A. G. Fowler, M. Mariantoni, J. M. Martinis, and A. N. Cleland, *Physical Review A* **86**, 10.1103/physreva.86.032324 (2012).
- [3] A. G. Fowler and C. Gidney, *Low overhead quantum computation using lattice surgery* (2019), arXiv:1808.06709 [quant-ph].
- [4] H. Zhou, C. Zhao, M. Cain, D. Bluvstein, C. Duckering, H.-Y. Hu, S.-T. Wang, A. Kubica, and M. D. Lukin, *Algorithmic fault tolerance for fast quantum computing* (2024), arXiv:2406.17653 [quant-ph].
- [5] B. Eastin and E. Knill, *Phys. Rev. Lett.* **102**, 110502 (2009).
- [6] S. Bravyi and R. König, *Phys. Rev. Lett.* **110**, 170503 (2013).
- [7] Y. Li, *New Journal of Physics* **17**, 023037 (2015).
- [8] L. Lao and B. Criger, *Magic state injection on the rotated surface code* (2022).
- [9] H. Bombín, M. Pant, S. Roberts, and K. I. Seetharam, *PRX Quantum* **5**, 010302 (2024).
- [10] C. Gidney, N. Shutty, and C. Jones, *Magic state cultivation: growing T states as cheap as CNOT gates* (2024), arXiv:2409.17595 [quant-ph].
- [11] S. Bravyi and A. Kitaev, *Phys. Rev. A* **71**, 022316 (2005).
- [12] S. Bravyi and J. Haah, *Physical Review A* **86**, 10.1103/physreva.86.052329 (2012).
- [13] J. Haah and M. B. Hastings, *Quantum* **2**, 71 (2018).
- [14] A. G. Fowler and S. J. Devitt, *A bridge to lower overhead quantum computation* (2013), arXiv:1209.0510 [quant-ph].

- ph].
- [15] D. Herr, F. Nori, and S. J. Devitt, *New Journal of Physics* **19**, 013034 (2017).
- [16] C. Gidney, *Quantum* **8**, 1310 (2024).
- [17] J. E. Moussa, *Phys. Rev. A* **94**, 042316 (2016).
- [18] N. P. Breuckmann and S. Burton, *Quantum* **8**, 1372 (2024).
- [19] With a catalyst  $|T\rangle$  state, the output state from a  $|CCZ\rangle$  factory can be transformed into two  $|T\rangle$  states [20].
- [20] C. Gidney and A. G. Fowler, *Quantum* **3**, 135 (2019).
- [21] L. Postler, F. Butt, I. Pogorelov, C. D. Marciniak, S. Heußen, R. Blatt, P. Schindler, M. Rispler, M. Müller, and T. Monz, Demonstration of fault-tolerant steane quantum error correction (2023), arXiv:2312.09745 [quant-ph].
- [22] C. Ryan-Anderson, J. G. Bohnet, K. Lee, D. Gresh, A. Hankin, J. P. Gaebler, D. Francois, A. Chernoguzov, D. Lucchetti, N. C. Brown, T. M. Gatterman, S. K. Halit, K. Gilmore, J. A. Gerber, B. Neyenhuis, D. Hayes, and R. P. Stutz, *Phys. Rev. X* **11**, 041058 (2021).
- [23] C. Ryan-Anderson, N. C. Brown, C. H. Baldwin, J. M. Dreiling, C. Foltz, J. P. Gaebler, T. M. Gatterman, N. Hewitt, C. Holliman, C. V. Horst, J. Johansen, D. Lucchetti, T. Mengle, M. Matheny, Y. Matsuo, K. Mayer, M. Mills, S. A. Moses, B. Neyenhuis, J. Pino, P. Siegfried, R. P. Stutz, J. Walker, and D. Hayes, High-fidelity and Fault-tolerant Teleportation of a Logical Qubit using Transversal Gates and Lattice Surgery on a Trapped-ion Quantum Computer (2024), arXiv:2404.16728 [quant-ph].
- [24] D. Bluvstein, S. J. Evered, A. A. Geim, S. H. Li, H. Zhou, T. Manovitz, S. Ebadi, M. Cain, M. Kalinowski, D. Hangleiter, J. P. Bonilla Ataides, N. Maskara, I. Cong, X. Gao, P. Sales Rodriguez, T. Karolyshyn, G. Semeghini, M. J. Gullans, M. Greiner, V. Vuletić, and M. D. Lukin, *Nature* **626**, 58 (2024).
- [25] R. Acharya, L. Aghababaie-Beni, I. Aleiner, T. I. Andersen, M. Ansmann, F. Arute, K. Arya, A. Asfaw, N. Astrakhantsev, J. Atalaya, R. Babbush, D. Bacon, B. Ballard, J. C. Bardin, J. Bausch, A. Bengtsson, A. Bिल्mes, S. Blackwell, S. Boixo, *et al.*, Quantum error correction below the surface code threshold (2024), arXiv:2408.13687 [quant-ph].
- [26] M. Webber, V. Elfving, S. Weidt, and W. K. Hensinger, *AVS Quantum Science* **4**, 10.1116/5.0073075 (2022).
- [27] M. Webber, S. Herbert, S. Weidt, and W. K. Hensinger, *Advanced Quantum Technologies* **3**, 2000027 (2020).
- [28] B. Lekitsch, S. Weidt, A. G. Fowler, K. Mølmer, S. J. Devitt, C. Wunderlich, and W. K. Hensinger, *Science Advances* **3**, 10.1126/sciadv.1601540 (2017).
- [29] M. Akhtar, F. Bonus, F. R. Lebrun-Gallagher, N. I. Johnson, M. Siegele-Brown, S. Hong, S. J. Hile, S. A. Kulmiya, S. Weidt, and W. K. Hensinger, *Nature Communications* **14**, 10.1038/s41467-022-35285-3 (2023).
- [30] M. Cain, C. Zhao, H. Zhou, N. Meister, J. P. B. Ataides, A. Jaffe, D. Bluvstein, and M. D. Lukin, *Phys. Rev. Lett.* **133**, 240602 (2024).
- [31] K. H. Wan, M. Webber, A. G. Fowler, and W. K. Hensinger, An iterative transversal CNOT decoder (2024), arXiv:2407.20976 [quant-ph].
- [32] D. Litinski, *Quantum* **3**, 205 (2019).
- [33] Double the qubit-cycles to include ancilla qubits [32].
- [34] Universal Quantum Ltd team, Transversal versus lattice surgery cnot (In preparation).
- [35] H. J. Briegel, D. E. Browne, W. Dür, R. Raussendorf, and M. Van den Nest, *Nature Physics* **5**, 19–26 (2009).
- [36] R. S. Gupta, N. Sundaresan, T. Alexander, C. J. Wood, S. T. Merkel, M. B. Healy, M. Hillenbrand, T. Jochym-O’Connor, J. R. Wootton, T. J. Yoder, A. W. Cross, M. Takita, and B. J. Brown, *Nature* **625**, 259–263 (2024).
- [37] in *The Error Correction Zoo*, edited by V. V. Albert and P. Faist (2024).
- [38] in *The Error Correction Zoo*, edited by V. V. Albert and P. Faist (2024).
- [39] M. E. Beverland, A. Kubica, and K. M. Svore, *PRX Quantum* **2**, 020341 (2021).
- [40] C. Gidney, M. Newman, and M. McEwen, *Quantum* **6**, 813 (2022).
- [41] V. V. Albert and P. Faist, eds., *The Error Correction Zoo* (2024).
- [42] C. Gidney, Cleaner magic states with hook injection (2023), arXiv:2302.12292 [quant-ph].
- [43] C. Gidney, *Quantum* **5**, 497 (2021).
- [44] O. Higgott and C. Gidney, PyMatching v2, <https://github.com/oscarhiggott/PyMatching> (2022).
- [45] M. McEwen, D. Bacon, and C. Gidney, *Quantum* **7**, 1172 (2023).
- [46] H. Bombin, D. Litinski, N. Nickerson, F. Pastawski, and S. Roberts, *Quantum* **8**, 1379 (2024).
- [47] B. Rodatz, B. Poór, and A. Kissinger, Floquetifying stabiliser codes with distance-preserving rewrites (2024), arXiv:2410.17240 [quant-ph].
- [48] B. Rodatz, B. Poór, and A. Kissinger, Fault tolerance by construction (2025), arXiv:2506.17181 [quant-ph].
- [49] M. Rüsçh, B. Rodatz, and A. Kissinger, Completeness for Fault Equivalence of Clifford ZX Diagrams (2025), arXiv:2510.08477 [quant-ph].
- [50] Without the conditional transversal  $S$  gates [4, 17? ? , 18].
- [51] A. Kissinger and J. van de Wetering, *Quantum Science and Technology* **7**, 044001 (2022).
- [52] Z.-H. Chen, M.-C. Chen, C.-Y. Lu, and J.-W. Pan, Efficient Magic State Cultivation on  $\mathbb{R}P^2$  (2025), arXiv:2503.18657 [quant-ph].
- [53] Y. Vaknin, S. Jacoby, A. Grimsmo, and A. Retzker, Magic State Cultivation on the Surface Code (2025), arXiv:2502.01743 [quant-ph].
- [54] S.-H. Lee, F. Thomsen, N. Fazio, B. J. Brown, and S. D. Bartlett, Low-overhead magic state distillation with color codes (2025), arXiv:2409.07707 [quant-ph].
- [55] S. Jacoby, Y. Vaknin, A. Retzker, and A. L. Grimsmo, Magic State Injection with Erasure Qubits (2025), arXiv:2504.02935 [quant-ph].
- [56] A. M. Dalzell, S. McArdle, M. Berta, P. Bienias, C.-F. Chen, A. Gilyén, C. T. Hann, M. J. Kastoryano, E. T. Khabiboulline, A. Kubica, G. Salton, S. Wang, and F. G. S. L. Brandão, Quantum algorithms: A survey of applications and end-to-end complexities (2023), arXiv:2310.03011 [quant-ph].
- [57] Creating a labeled tetrahedron with tikzpicture, <https://tex.stackexchange.com/questions/174317>, accessed: 2024-10-21.
- [58] A. Kissinger and J. van de Wetering, in *Proceedings 16th International Conference on Quantum Physics and Logic, Chapman University, Orange, CA, USA., 10-14 June 2019*, Electronic Proceedings in Theoretical Computer Science, Vol. 318, edited by B. Coecke and M. Leifer (Open Publishing Association, 2020) pp. 229–241.



## Appendix A: Figures of merit and benchmarking logical failure

It may be more convenient to use ZX-calculus [59] and Pauli webs [47–49] to represent the stabiliser structures of the logical distillation circuits studied in the main text; and to benchmark their corresponding stabiliser proxies ofr logical error rate analysis. Below we shall briefly describe how to map the 7-to-1 protocol’s quantum circuit to its ZX-diagram, before illustrating how Pauli webs can be used to benchmark the logical error rate of this protocol.

### 1. Translations from quantum circuit to ZX-diagram

The following equations (equation A1 to A9) represent the mapping of quantum circuit diagrams to ZX-gadgets. Namely, CNOT, various Clifford state initialisation and measurements with specific outcomes.

$$\text{CNOT} = \begin{array}{c} \text{---} \text{---} \text{---} \\ \text{---} \text{---} \text{---} \end{array} \quad (A1)$$

$$|0\rangle \propto \text{---} \text{---} \quad (A2)$$

$$|+\rangle \propto \text{---} \text{---} \quad (A3)$$

$$|1\rangle \propto \text{---} \text{---} \quad (A4)$$

$$|-\rangle \propto \text{---} \text{---} \quad (A5)$$

$$|Y\rangle \propto \text{---} \text{---} \quad (A6)$$

$$S = \text{---} \text{---} \quad (A7)$$

$$\text{---} \boxed{\text{---}} = n_j \in \{0, 1\} \rightarrow \text{---} \text{---} \quad (A8)$$

$$\text{---} \boxed{M_X} = m_j \in \{0, 1\} \rightarrow \text{---} \text{---} \quad (A9)$$

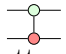
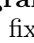
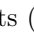


Along with the non-Clifford  $T$  gate and  $|T\rangle$  state.

$$|T\rangle \propto \text{---} \text{---} \quad (A10)$$

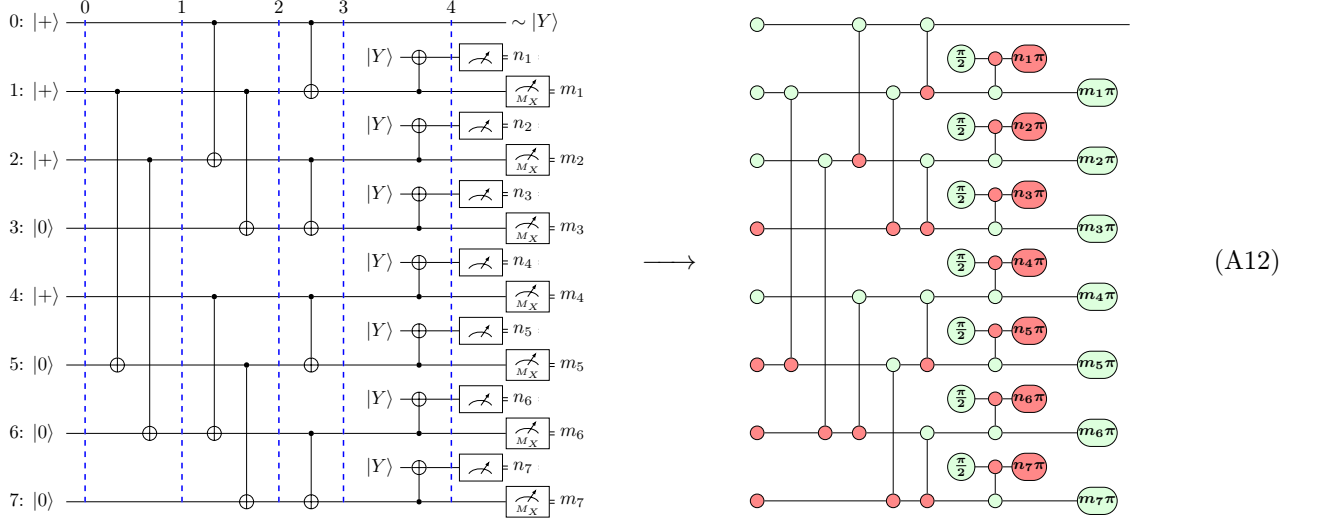
$$T = \text{---} \text{---} \quad (A11)$$

### 2. ZX-diagram interpretation for the 7-to-1 $|Y\rangle$ protocol

ZX-calculus provides a convenient bookkeeping language for stabiliser structure (including CNOT circuits, Pauli state preparations, and Pauli measurements) for quantum circuits represented as ZX-diagrams. In our case, the 7-to-1 protocol can be viewed as a Clifford entangling circuit that prepares a Bell pair between the output patch 0 and an encoded Steane block (patches 1, ..., 7), followed by a transversal  $S$  on the Steane block implemented by  $|Y\rangle$ -state consumption, and finally  $X$ -basis readout of the Steane code. The resulting quantum circuit to ZX-diagram mapping in equation A12 shows:

- CNOT layers  $\rightarrow$  connected graph.** Each CNOT corresponds to a fixed ZX gadget (  , see equation A1), and the three parallel CNOT layers of figure 2 translate to a purely graphical wiring pattern among vertices.
- State preparations and measurements  $\rightarrow$  boundary conditions of the ZX-diagram.** The initialisations  $|+\rangle$  (  ) and  $|0\rangle$  (  ) correspond to boundary vertices (equation A3 and A2) which fix the stabilisers at the input of the circuit. Similarly, the final  $Z$ - (  ) and  $X$ -basis (  ) measurements (equation A8 and A9) terminate wires and generate measurement outcomes  $n_j$  and  $m_j$ .

3.  $|Y\rangle$  ( $\frac{\pi}{2}$ -) consumption realises a transversal  $S$  ( $-\frac{\pi}{2}$ -) on patches 1 to 7. Consuming  $|Y\rangle$  via the teleportation gadget (equation A6 with a CNOT and  $Z$  measurement) implements  $S$  up to a Pauli byproduct conditioned on the measurement outcome.



### 3. Pauli webs for 7-to-1 distillation protocol

Pauli webs [46] (also called stabiliser flows for quantum circuits [45]) are decorations on Clifford ZX-diagrams, providing a compact description of how a Pauli observable “propagates” through a Clifford circuit. Or in other words, it reveals the underlying stabiliser structure of the corresponding ZX-diagram/resultant quantum state. As an example, the 3-GHZ state with a single  $S$  gate applied ( $SII(|000\rangle + |111\rangle)$ ) can be represented as the following ZX-diagram with the following stabiliser generators:

$$\left( \frac{\pi}{2} \right) \text{---} \propto SII(|000\rangle + |111\rangle), \quad \langle ZZI, IZZ, YXX \rangle, \quad (\text{A13})$$

where the following open Pauli webs (edge highlights) describe its stabilisers of this state at the boundary of the ZX-diagram (Pauli- $XYZ$  coloured accordingly).

$$\left\langle \left( \frac{\pi}{2} \right) \text{---} \overset{Z}{\curvearrowright} \text{---} \overset{Z}{\curvearrowright} \text{---} \left( \frac{\pi}{2} \right) \text{---} \overset{Z}{\curvearrowright} \text{---} \left( \frac{\pi}{2} \right) \text{---} \overset{Z}{\curvearrowright} \text{---} \left( \frac{\pi}{2} \right) \text{---} \right\rangle, \quad \langle ZZI, IZZ, YXX \rangle \quad (\text{A14})$$

For the 7-to-1 protocol's ZX-diagram, there are four Pauli webs, shown in equation A15. These are the logical Pauli webs, where each subsystem corresponds to a surface code patch in our case.

logical  $Y$  membrane
 $X_1X_3X_5X_7$ 
 $X_2X_3X_6X_7$ 
 $X_4X_5X_6X_7$

(A15)

- **Logical  $Y$ .** The web labelled “Logical  $Y$  membrane” is the Pauli web/stabiliser flow corresponding to the desired output stabiliser on patch 0 (for  $|Y\rangle$  distillation, the target is  $Y_0$  up to a known sign). The sign of the output stabiliser depends on a global parity of the classical outcomes, as shown in the boundary of these Pauli webs:

$$Y_0 \mapsto (-1)^{1+\sum_{k=1}^7(m_k+n_k)} Y_0, \quad (\text{A16})$$

matching equation 6. In practice, we track this sign as a Pauli-frame update (or equivalently, a potential  $Z_0$  correction), rather than applying a physical correction.

- **Steane code  $X$ -stabiliser check Pauli webs.** The remaining three webs in equation A15 correspond to the three independent weight-4 Steane  $X$  stabilisers. In terms of the measurement outcomes, the three parities are

$$s_{1357} = (m_1 \oplus n_1) \oplus (m_3 \oplus n_3) \oplus (m_5 \oplus n_5) \oplus (m_7 \oplus n_7), \quad (\text{A17})$$

$$s_{2367} = (m_2 \oplus n_2) \oplus (m_3 \oplus n_3) \oplus (m_6 \oplus n_6) \oplus (m_7 \oplus n_7), \quad (\text{A18})$$

$$s_{4567} = (m_4 \oplus n_4) \oplus (m_5 \oplus n_5) \oplus (m_6 \oplus n_6) \oplus (m_7 \oplus n_7). \quad (\text{A19})$$

The post-selection rule is simply

$$s_{1357} = s_{2367} = s_{4567} = 0, \quad (\text{A20})$$

equivalent to checking for all the Steane code  $X$ -stabiliser check Pauli webs to be unviolated.

#### 4. Benchmarking the 7-to-1 protocol and logical failure

A Pauli web corresponds to a Pauli observable propagated through the circuit. Two webs that differ by multiplication with a check web (namely a stabiliser flow that is fixed to  $+1$  upon post-selection) represent the same logical observable. This is the analogue of multiplying a logical operator by a stabiliser in a stabiliser code. In the 7-to-1 protocol, post-selection enforces the three Steane  $X$ -checks in equation A19 to be trivial. Consequently, the logical- $Y$  membrane web in equation A15 can be freely multiplied by any of the three check webs without changing its action on the codespace. Multiplying the logical  $Y$  membrane by the  $X_4X_5X_6X_7$  web yields an equivalent, smaller weight Pauli web representation:

(A21)

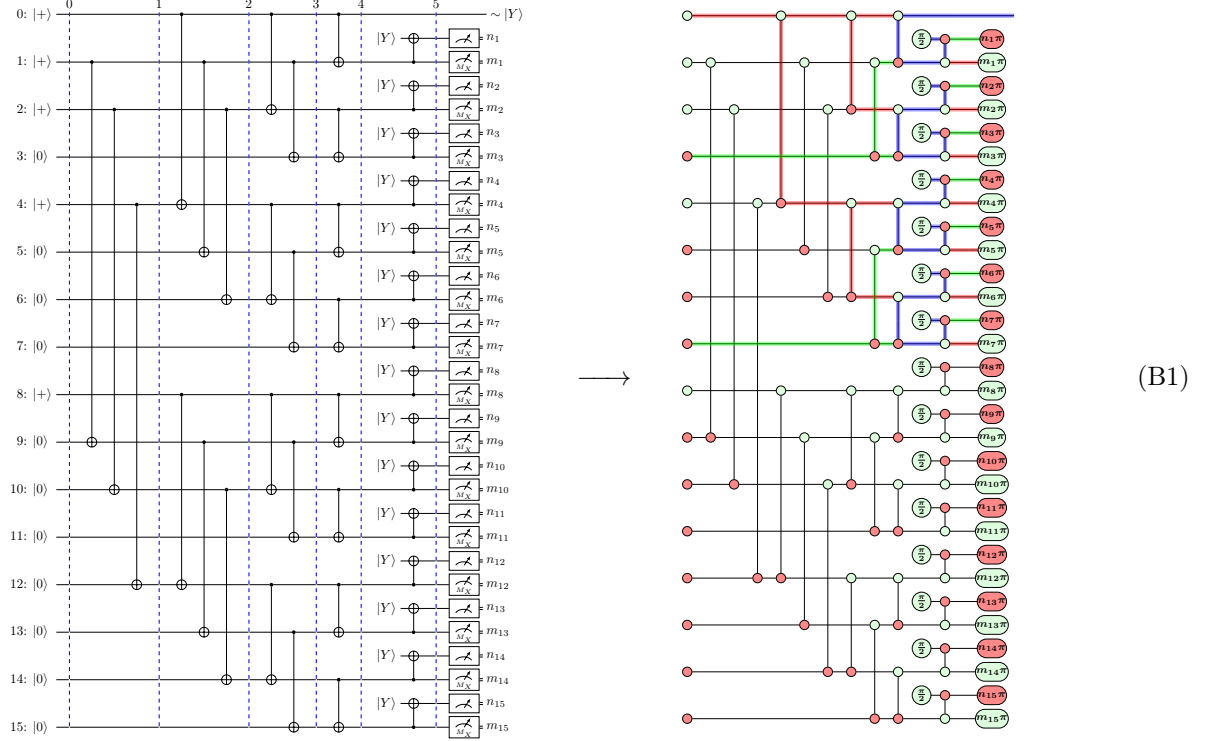
We may benchmark this stabiliser circuit by estimating the post-selected logical failure rate on the output patch 0. For each sampled shot, we:

1. decode all surface-code patches (iteratively, when transversal CNOTs are present) to obtain logical measurement outcomes ( $m_j$ ) and consumption outcomes ( $n_j$ ), together with a consistent Pauli frame, then
2. apply the post-selection rule:  $s_{1357} = s_{2367} = s_{4567} = 0$  from equation A20,
3. for accepted shots, then compute the predicted sign of the output  $Y_0$  stabiliser using the global parity in equation A16 (equivalently, update the output Pauli frame by the corresponding Clifford correction), and finally
4. declare a logical failure if the decoded output is inconsistent with the target  $|Y\rangle$  eigenvalue after applying the tracked frame update.

Or alternatively, if the Pauli web on the LHS of equation A21 is violated, then it implies a logical error.

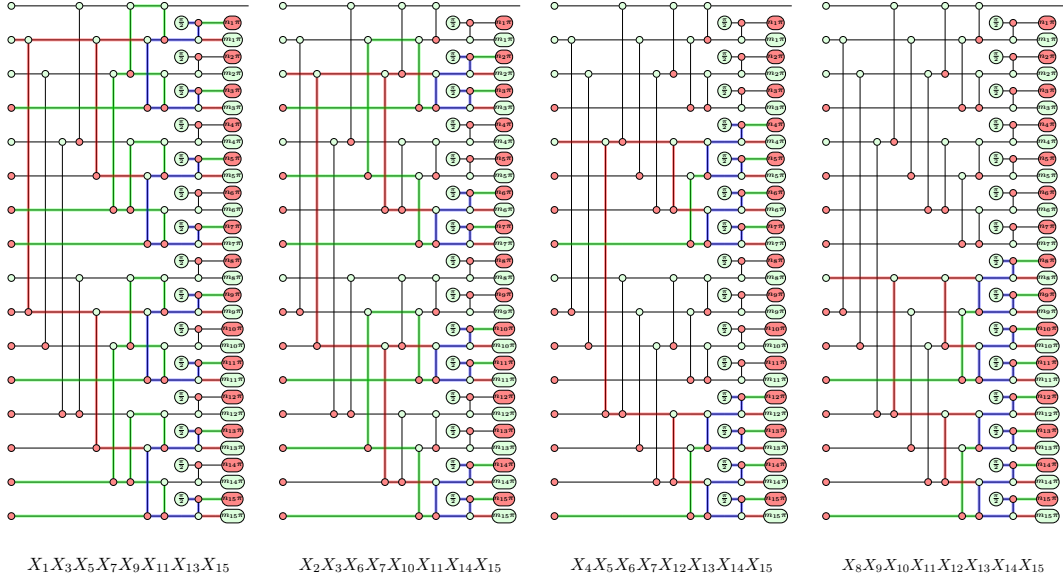
**Appendix B: Benchmarking the stabiliser proxy to the 15-to-1 protocol**

The 15-to-1 protocol is a non-Clifford distillation routine when implemented with  $|T\rangle$  state consumptions, hence direct large distance end to end simulation is challenging. Instead, one can benchmark a stabiliser proxy obtained by replacing all the non-Clifford resource state by a Clifford state (for example,  $|Y\rangle$  states are consumed, shown in equation B1), implementing a transversal  $S$  up to Pauli byproducts. This retains a similar CNOT encoding sub-circuit and, crucially, preserves a similar post-selection structure based on Reed-Muller  $X$ -stabiliser checks.



In the Pauli web language, the proxy circuit admits four independent weight-8 Reed-Muller code  $X$ -type stabilisers as Pauli webs (see equation B2) and one logical membrane web supported on the output of patch 0 (shown on the RHS of equation B1). We post-select on the trivial values of all four  $X$ -check webs, and then track the Pauli-frame on patch 0. Conditioned on successful post-selection, a logical failure occurs when the logical membrane web is violated

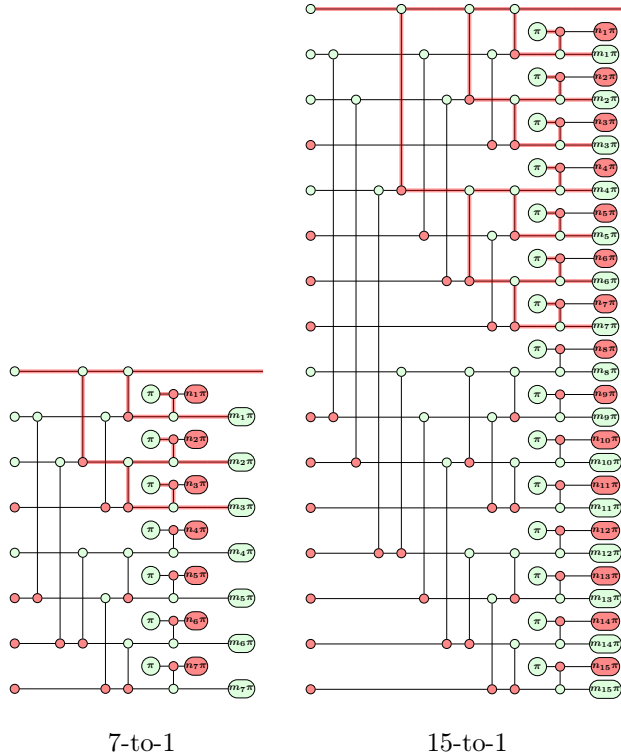
(equivalently, the decoded output is inconsistent with the target stabiliser sign after Pauli frame update).



(B2)

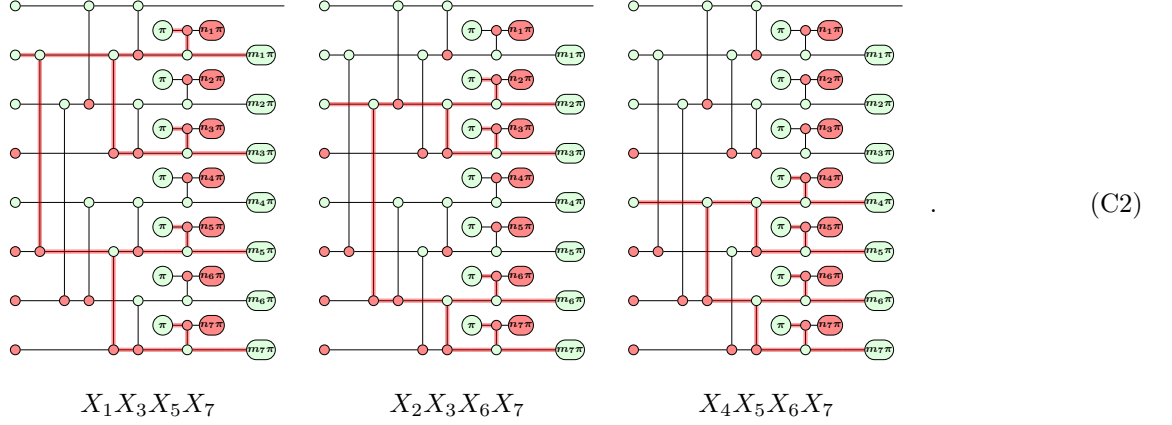
**Appendix C: Pauli web simulation proxies used in main text**

In the main text we benchmark both the 7-to-1 and 15-to-1 circuits using a stabiliser proxy based on distilling  $|-\rangle$  (and injecting  $Z$  faults with probability  $p$  on the consumed resource states). This proxy isolates the post-selection and decoding behaviour of the factory and allows us to confirm the expected cubic suppression scaling under circuit-level noise. See below (equation C1) for the logical membranes of the  $|-\rangle$  state proxies to the 7-to-1 and 15-to-1 protocols.

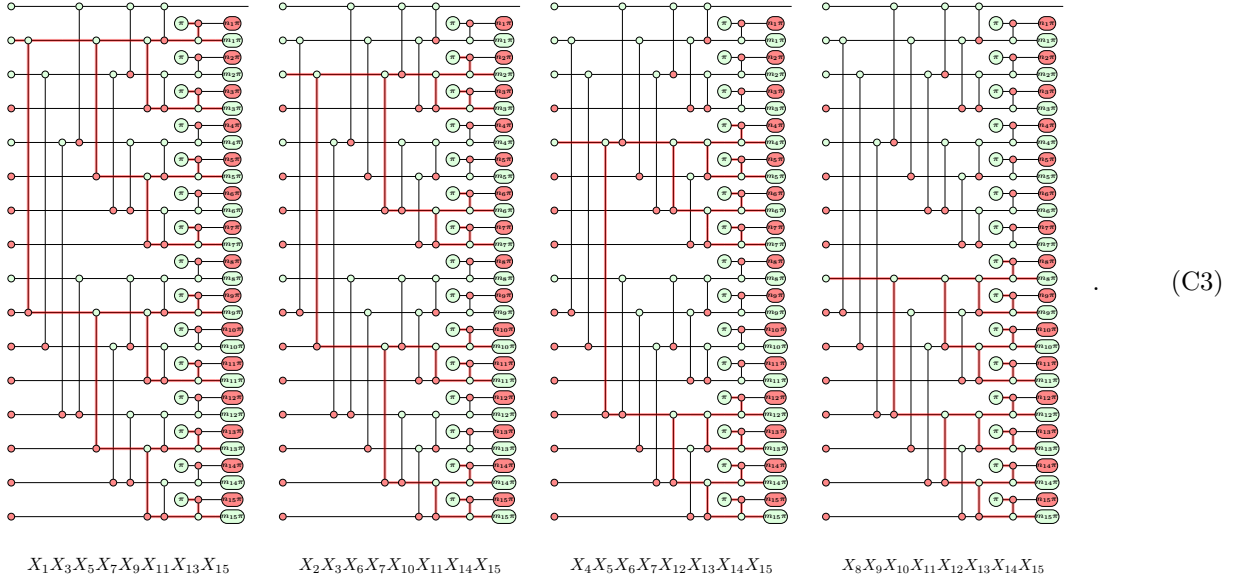


(C1)

Post-selecting on the following logical check webs for the 7-to-1 protocol,



And for the 15-to-1 protocol, post-selecting on the following logical check webs:



For either distillation circuits, these stabiliser proxies access only the logical  $X$  initialisation and measurement outcomes.